IEEE Transactions on Nuclear Science, Vol. NS-26, No. 3, June 1979

COMPUTER CALCULATIONS OF TRAVELING-WAVE PERIODIC STRUCTURE PROPERTIES*

G.A. Loew, R.H. Miller, R.A. Early
and K.L. Bane

Stanford Linear Accelerator Center
Stanford University, Stanford, California 94305

Introduction

The versatility and accuracy of programs such as LALA[1] and specially SUPERFISH[2] to calculate the rf properties of standing-wave cavities for linacs and storage rings is by now well established. Such rf properties include the resonant frequency, the phase shift per periodic length, the E- and H-field configurations, the shunt impedance per unit length and Q. While other programs such as TWAP[3] have existed for some time for traveling-wave structures, the wide availability of SUPERFISH makes it desirable to extend the use of this program to traveling-wave structures as well. That is the purpose of this paper. In the process of showing how the conversion from standing waves to traveling waves can be accomplished and how the group velocity can be calculated, the paper also attempts to clear up some of the common ambiguities between the properties of these two types of waves. Good agreement is found between calculated results and experimental values obtained earlier.

Space Harmonics, Standing and Traveling Waves

To illustrate our problem, let us review the case of the classical cylindrically symmetric disk-loaded waveguide for which LALA and SUPERFISH can yield exact field solutions. It is well known[4] that in the lowest pass-band (accelerating TM_{01}-type mode), the traveling-wave E_z field can be expressed as

$$E_{z,TW} = \sum_{n=-\infty}^{n=+\infty} a_n J_o(k_{rn} r) e^{j(\omega t - \beta_n z)} \qquad (1)$$

where a_n is the amplitude of the space harmonic of index n, $\beta_n z = \beta_o z + 2\pi nz/d$, $k_{rn}^2 = k^2 - \beta_n^2$, $k = \omega/c$ and d is the periodic length. Let a be the radius of the iris and b the radius of the cylinder. On axis r = o, $J_o(0) = 1$ and the amplitudes all reduce to the a_n's. Furthermore, the fundamental (n = 0) field amplitude at any r, for a structure where $\beta_o = k = \omega/c$ is equal to $a_oJ_o(0)$, which indicates that a synchronous electron undergoes the same average acceleration independently of radial position. If one chooses the origin at a point of symmetry of the structure (in the middle of a cavity or a disk) the a_n's are all real. Notice that for r = 0, expression (1) assumes a special form when z = 0 and when z = d/2:

$$z = 0 \quad E_z = e^{j\omega t}\Sigma a_o + a_{-1} + a_{+1} + a_{+2} + a_{-2} + \dots$$
$$z = \frac{d}{2} \quad E_z = e^{(\omega t - \beta_o \frac{d}{2})}\Sigma a_o - a_{-1} - a_{+1} + a_{+2} + a_{-2} + \dots \qquad (2)$$

i.e., the axial traveling-wave E-field goes through an extremum where all the space harmonics are colinear. This is also how at r = a the space harmonics "conspire" to make the tangential E-field at the disk edge equal to zero, i.e., how they fulfill the function for which they were invented in the first place, namely to match periodic boundary conditions. Notice also that if the phase shift per cell is an exact sub-multiple of 2π, i.e., $\beta_o d = 2\pi/m$, then $\beta_n = \beta_o(1 + mn)$. In what follows, we will focus on the so-called $2\pi/3$ mode (m = 3) which is easy to represent schematically and for which there is a large amount of experimental data from the SLAC linac and many others. The results, however, are quite general and apply to any $\beta_o d$ except π. Fig. 1a illustrates the behavior of E_z, E_r and H_ϕ: two traveling-wave snapshots of E are shown for two instants of time, $\omega t = 0$ and $\omega t = \pi/2$. Notice that E_z is plotted on axis (r = 0) but E_r and H_ϕ are zero on axis and thus are plotted for $0 < r < a$. The units are arbitrary. The field patterns that are shown have for many years been known approximately from bead measurements, paraxial approximations of Maxwell's equations and general symmetry arguments. However, some of the subtleties in Fig. 1a can only be gotten from a complete computer solution, as shown later in this paper. Notice also that since the fields are sketched at an instant of time, they are not at their maxima, except for selected symmetry planes. H_ϕ travels in phase with E_r to preserve a net power flow $(E \times H)_z = E_r H_\phi$. Fig. 1b shows $E_{z,TW}$ max at r = 0 vs z and the corresponding phase variation, as governed by Eq. (1).

The standing waves are shown in Fig. 1c. The snapshots of E are given for two different boundary conditions: Neuman ($E_T = 0$) on the left, and Dirichlet ($H_T = 0$) on the right. E_z and E_r which are shown at their maximum values in time are in time-phase, H_ϕ leads them in time quadrature and there is no power propagation: the energy simply switches back and forth between the electric and magnetic fields. On the axis (r = 0), the axial electric fields can be expressed as:

$$E_{z,SW} = e^{j\omega t}\sum_{n=-\infty}^{n=+\infty} 2a_n \cos\beta_n z \quad \text{(Neuman)} \qquad (3)$$

$$E_{z,SW} = e^{j\omega t}\sum_{n=-\infty}^{n=+\infty} 2a_n \sin\beta_n z \quad \text{(Dirichlet)} \qquad (4)$$

where the factor of 2 comes from the summation of two traveling waves of amplitude a_n. These and the corresponding E_r and H_ϕ are the components calculated by LALA and SUPERFISH. Notice that the snapshots of $E_{z,TW}$ and $E_{z,SW}$ at the instants chosen are indistinguishable but H_ϕ is different.

Group Velocity

The group velocity for a traveling wave can be obtained from the dispersion diagram ($v_g = d\omega/d\beta$) or from the energy velocity ($v_g = P/W_{TW}$) where P is the power flow and W_{TW} is the energy stored per unit length. In order to calculate v_g with some accuracy from the first expression, which is generally done for the standing-wave case, one needs to compute several frequencies on the $\omega - \beta_o d$ diagram, typically for $\beta_o d = 0, \pi/3, \pi/2, 2\pi/3$ and π, and then fit the data to some smooth curve. If however we want to obtain v_g by calculating the fields at only one frequency, namely the operating frequency, then the second expression is to be used. For a given z, we have:

$$v_g = \frac{P}{W_{TW}} = \frac{\frac{1}{2}\int E_r H_\phi \, dS}{\int_{\substack{\text{unit}\\\text{length}}} \frac{\epsilon E^2}{2} dV + \int_{\substack{\text{unit}\\\text{length}}} \frac{\mu H^2}{2} dV} \qquad (5)$$

*Work supported by the Department of Energy under contract number EY-76-C-03-0515.

0018-9499/79/0600-3701$00.75 © 1979 IEEE

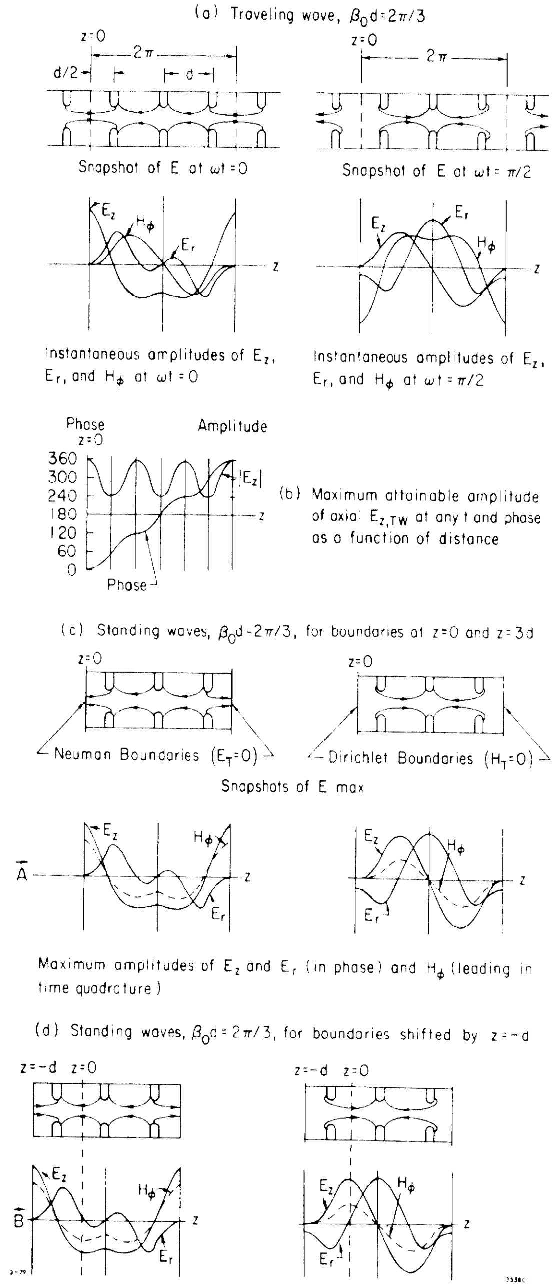

Figure 1

It turns out that LALA and SUPERFISH already give W_{SW}, the energy stored for the SW case. The denominator W_{TW} is simply $W_{SW}/2$: this can be shown rigorously or seen by superposition since over a wavelength, the energy stored from a TW coming from the left added to that from a TW coming from the right results in twice the energy stored. The expression in the numerator can in principle be calculated at any cross-sectional plane (S) since, by continuity, energy cannot accumulate and the net power flow over a period must be independent of the plane of integration. What we need to know are the simultaneous values of $E_{r,TW}$ and $H_{\phi,TW}$ at their time maxima in one plane. These quantities can be extracted from the SW plots. To do so, a "trick" is needed. If two traveling waves of the proper phase add up to a standing wave (Eqs. (3), (4)), there must conversely be two standing waves which add up to a traveling wave. Referring to Fig. 1d, we see that if for example we shift the diagram of Fig. 1c to the left by $z=-d$, we have a second SW solution ($\vec{B}$) which looks just like the first one ($\vec{A}$):

$$\vec{B} = e^{j\omega t}\sum_{-\infty}^{+\infty} 2a_n \cos\beta_n (z+d)$$
$$\vec{A} = e^{j\omega t}\sum_{-\infty}^{+\infty} 2a_n \cos\beta_n z \qquad (6)$$

both of which are made up of one TW going left and one going right. The "trick" is to add them with the proper phases to have the TW's going left cancel and those going right add. This can be achieved by multiplying $\vec{A}$ by $e^{j(\beta_0 d - \pi/2)}$ and $\vec{B}$ by $e^{j\pi/2}$. Then:

$$A e^{j(\beta_0 d - \frac{\pi}{2})} + B e^{j\frac{\pi}{2}} = 2\sin\beta_0 d \underbrace{\sum_{-\infty}^{+\infty} a_n e^{j(\omega t - \beta_n z)}}_{TW}$$

and it follows that the amplitude and phase of the TW are:

$$|TW|^2 = \frac{A^2 + B^2 - 2AB\cos\beta_0 d}{4\sin^2\beta_0 d} \qquad (7)$$

$$\tan\theta(z) = \frac{B - A\cos\beta_0 d}{A\sin\beta_0 d} \qquad (8)$$

where A and B are functions of z. Eqs. (7),(8) are general and apply to any field component, E_r, E_z or H_ϕ, at any z. Hence, given exact SW field values, e.g., as shown in Fig. 2a and 2b, one can now obtain exact TW plots as in Fig. 1b. Eq. (7) gives the maximum TW amplitude at any z and thus yields the E_r and H_ϕ's needed for Eq. (5). Notice furthermore that Eqs. (7) and (8) can be obtained from $\vec{A}$ and $\vec{B}$ plots in either the Neuman or Dirichlet configurations. In what follows, we shall narrow down the discussion to planes of symmetry halfway through a cavity or a disk where Eqs. (7) and (8) are simplified.

Neuman case: With the Neuman boundaries of Fig. 1c, we see that $E_{r,SW}=0$ at $z=0$ and $3d/2$ but has finite values at $z=d/2$ and d. At $z=d/2$, $B=0$ and $E_{r,TW} = E_{r,SW}(d/2)/\sqrt{3}$. At $z=3d/2$, $B=-A$ and $E_{r,TW}=E_{r,SW}(3d/2)/\sqrt{3}$. Similar observations can be made for H_ϕ. For example, at $z=0$, $B=A\cos\beta_0 d$ and $H_{\phi,TW}=H_{\phi,SW}(0)/2$ and at $z=d$, $B=A$ and $H_{\phi,TW}=H_{\phi,SW}(d)$. The results are summarized in Table I. Since the tabulated values are the maxima of the fields, the results must be self-consistent and independent of which mid-cavity or disk one considers. For the power calculation, we can take the power flow at $z=d/2$, i.e., $E_{r,TW}H_{\phi,TW}=E_{r,SW}(d/2)\,H_{\phi,SW}(d/2)/\sqrt{3}$ or at $z=d$, i.e., $E_{r,TW}H_{\phi,TW}=E_{r,SW}(d)\,H_{\phi,SW}(d)/\sqrt{3}$.

Dirichlet case: Table II shows very similar results for the Dirichlet case shown in Fig. 1c.

Results

Table III shows the results that have been obtained by computing the properties of four SLAC-type cavities and by comparing them with results obtained experimentally[5] in the early 1960's. The four cavities whose 2b and 2a dimensions are shown are equally spaced along a constant-gradient 3.05 m section. The computed values of r/Q, Q and r are obtained from the standing-wave SUPERFISH calculations. The values of r/Q for the TW case are simply twice those for the SW case. All values of r/Q and r have been corrected for the a_0 (velocity of light) space harmonic amplitude. The values of Q are the same for the SW and the TW cases. The assumed conductivity of copper is 5.8×10^7 mhos/m. We see that in general, agreement between computed and experimental results is excellent. For reasons not understood, the resonant frequency is almost systematically high by 1 MHz. Most other differences including those for the group

Table I

Maximum Values of E_r and H_ϕ for Neuman Boundaries

Location	Mid-Cavity	Disk	Mid-Cavity	Disk
z	0	$\frac{d}{2}$	d	$\frac{3d}{2}$
$E_{r,SW}$	0	Finite	Finite	0
$E_{r,TW}$		$\frac{E_{r,SW}(\frac{d}{2})}{\sqrt{3}}$	$\frac{E_{r,SW}(d)}{\sqrt{3}}$	
$H_{\phi,SW}$	Finite	Finite	Finite	Finite
$H_{\phi,TW}$	$\frac{H_{\phi,SW}(0)}{2}$	$H_{\phi,SW}(d)$	$H_{\phi,SW}(d)$	$\frac{H_{\phi,SW}(\frac{3d}{2})}{2}$

Table II

Maximum Values of E_r and H_ϕ for Dirichlet Boundaries

Location	Mid-Cavity	Disk	Mid-Cavity	Disk
z	0	$\frac{d}{2}$	d	$\frac{3d}{2}$
$E_{r,SW}$	Finite	Finite	Finite	Finite
$E_{r,TW}$	$\frac{E_{r,SW}(0)}{2}$	$E_{r,SW}(\frac{d}{2})$	$E_{r,SW}(d)$	$\frac{E_{r,SW}(\frac{3d}{2})}{2}$
$H_{\phi,SW}$	0	Finite	Finite	0
$H_{\phi,TW}$		$\frac{H_{\phi,SW}(\frac{d}{2})}{\sqrt{3}}$	$\frac{H_{\phi,SW}(d)}{\sqrt{3}}$	

Table III

Comparison of Computed and Experimental Results for Four SLAC Cavities

Cavity No.	2b (cm)	2a (cm)	f_{exp} MHz	f_{comp} MHz	$(r/Q)_{exp}$ Ω/cm	$(r/Q)_{comp}$ Ω/cm	Q_{exp}	Q_{comp}	r_{exp} MΩ/m	r_{comp} MΩ/m	$(v_g/c)_{exp}$	$(v_g/c)_{comp}$
Neuman Boundaries												
1	8.3442	2.6201	2856	2857.04	38.13	38.99	14160	13780	54	53.7	0.0202	0.0204
28	8.2960	2.4506	2856	2857.74	40.40	40.70	13860	13760	56	56	0.0157	0.0161
57	8.2393	2.2185	2856	2857.40	42.77	43.08	13560	13736	58	59.2	0.0111	0.0113
84	8.1773	1.9171	2856	2857.15	45.45	46.07	13200	13710	60	63.2	0.0067	0.0073
Dirichlet Boundaries												
1	8.3442	2.6201	2856	2857.01	38.13	38.70	14160	13780	54	53.4	0.0202	0.0204
28	8.2960	2.4506	2856	2857.28	40.40	40.40	13860	13759	56	55.6	0.0157	0.0162
57	8.2393	2.2185	2856	2856.83	42.77	42.76	13560	13734	58	58.8	0.0111	0.0114
84	8.1773	1.9171	2856	2856.56	45.45	45.79	13200	13708	60	62.80	0.0067	0.0066

velocity, are within 1 or 2%. It should also be remembered that the experimental results were certainly not accurate to more than 2%. Slight discrepancies between the Neuman and Dirichlet results can be used as final checks to verify the ultimate reliability of the field calculations. Figs. 2a and b give actual computer plots of the maximum amplitude standing-wave snapshots shown in Fig. 1c. Both examples were computed for the dimensions of the first cavity in Table III. The periodic length d is 3.5 cm and the disk thickness 0.584 cm. All field amplitudes are in arbitrary units, E_z being on axis, E_r and H_ϕ off axis.

References

1. H.C. Hoyt, "Designing Resonant Cavities With the LALA Computer Program," Proc. of the 1966 Linear Accelerator Conf., Los Alamos Scientific Laboratory, New Mexico, Oct. 3-7, 1966, pp. 119-124.

2. K. Halbach, et al. "Properties of the Cylindrical RF Cavity Evaluation Code SUPERFISH," Proc. of the 1976 Proton Linear Accelerator Conf., Chalk River Nuclear Laboratories, Chalk River, Ontario, Sept. 14-17, 1976, pp. 122-128.

3. R.H. Helm, "Computation of the Properties of Traveling-Wave Linac Structures," Proc. of the 1970 Proton Linear Accel. Conf., National Accelerator Laboratory, Batavia, Illinois, Sept 28 - Oct. 2, 1970, Vol. I, pp. 279-291.

4. For earlier discussions on the subject treated in this paragraph, see P.M. Lapostolle and A.L. Septier "Linear Accelerators," North-Holland Pub. Co., Amsterdam (1970), pp. 40-47 and 88-107.

5. R.B. Neal, D. W. Dupen, H.A. Hogg, G.A. Loew, "The Stanford Two-Mile Accelerator," W.A. Benjamin, Inc., New York-Amsterdam (1968), p. 130, Fig. 6-22.

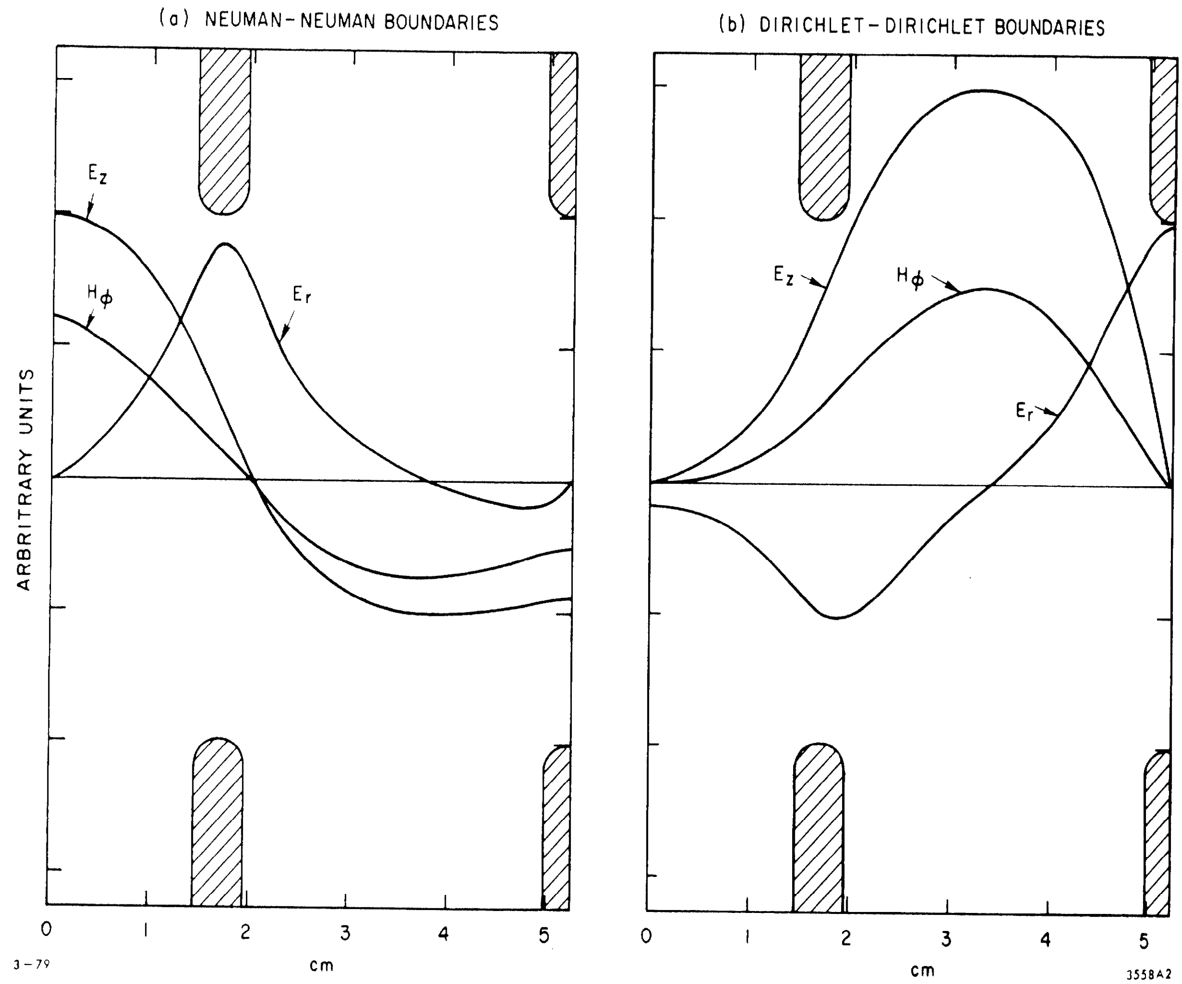

Fig. 2. Standing-wave amplitudes of E_z, E_r and H_ϕ in cavity (1) (see Table III) as calculated by SUPERFISH. E_z is on-axis, E_r and H_ϕ are off-axis.